

Search for Right-Handed Currents in Muon Decay

J. Carr, G. Gidal, B. Gobbi,^(a) A. Jodidio, C. J. Oram,^(b) K. A. Shinsky, H. M. Steiner,
D. P. Stoker, M. Strovink, and R. D. Tripp

Lawrence Berkeley Laboratory and Department of Physics, University of California, Berkeley, California 94720

(Received 8 June 1983)

New limits are reported on right-handed currents, based on precise measurement of the e^+ spectrum end point in μ^+ decay. Highly polarized muons from the TRIUMF "surface" beam were stopped in metal foils within a 1.1-T spin-holding longitudinal field or a 70-G spin-precessing transverse field. For the spin-held data, the $V-A$ decay rate vanishes in the beam direction at the end point. Measurement of this rate sets the 90%-confidence limits $\xi P_\mu \delta / \rho > 0.9959$ and $M(W_R) > 380$ GeV, where W_R is the possible right-handed gauge boson.

PACS numbers: 13.35.+s, 12.30.Ez, 14.60.Ef, 14.80.Er

If the $SU(2)_L \otimes U(1)$ gauge group in the standard electroweak model is extended, e.g., to $SU(2)_L \otimes SU(2)_R \otimes U(1)$,¹ left-right symmetry at the Lagrangian level is restored with the addition of a right-handed gauge boson W_R . The dominance of left-handed charged currents at present energies could then arise from a $W_L - W_R$ mass splitting which is tiny on the grand-unification scale. In these left-right symmetric theories, the physical bosons W_1 and W_2 , with mass-squared ratio $\alpha = M^2(W_1)/M^2(W_2)$, are $W_1 = W_L \cos \zeta - W_R \sin \zeta$ and $W_2 = W_L \sin \zeta + W_R \cos \zeta$. Analyses^{2,3} which neglect the kinematic effect of any ν_R mass obtain the strongest limits on α and the mixing angle ζ from muon and nucleon β decay.⁴⁻⁹ Additional constraints are placed by model-dependent calculations, e.g., of the $K_L^0 - K_S^0$ mass difference.¹⁰ Present experimental bounds are displayed in Fig. 1. We present here a precise measurement of the high-momentum region of the e^+ spectrum in polarized μ^+ decay, resulting in the new limit given by the small bold ellipse in Fig. 1.

The stopped μ^+ decays of interest are those which emit e^+ near the momentum-spectrum end point $x = p_e/p_e(\text{max}) = 1$, and also near $\theta = 0$, where $\pi - \theta$ is the angle between \hat{p}_e and the direction of μ^+ polarization P_μ . Relative to that for unpolarized muons, the decay rate is

$$R(x, \theta) = 1 - \frac{1 - 2\tilde{x} - \tilde{\delta} + 4\tilde{x}\tilde{\delta}}{1 + 2\tilde{x} - \tilde{\rho} + 4\tilde{x}\tilde{\rho}} \xi P_\mu \cos \theta, \quad (1)$$

where $\tilde{x} = 1 - x$, $\tilde{\delta} = 1 - 4\delta/3$, $\tilde{\rho} = 1 - 4\rho/3$, and ξ , δ , and ρ are the usual muon-decay parameters.¹¹ [Radiative corrections¹¹ and the finite electron mass are included in the actual analysis but neglected in (1) above.] At the end point, $R(1, 0) = 1 - \xi P_\mu \delta / \rho$, and in the $V-A$ limit, $R(x \rightarrow 1, \theta \rightarrow 0) \approx 6 - 4x - P_\mu - \cos \theta$. For a μ^+ beam derived from π^+ decay at rest, θ becomes the angle between the e^+ and μ^+ momenta. Then, in left-right sym-

metric theories,² $P_\mu \approx 1 - 2(\alpha + \zeta)^2$, and the end-point decay rate $R(1, 0) \approx 2(2\alpha^2 + 2\alpha\zeta + \zeta^2)$ con-

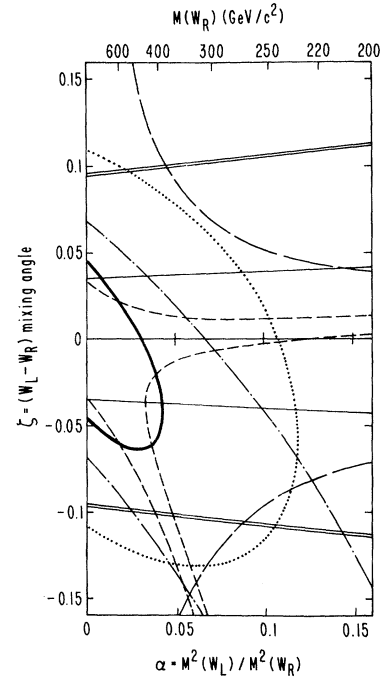


FIG. 1. Experimental 90%-confidence limits on the $W_L - W_R$ mass-squared ratio α and mixing angle ζ describing possible right-handed charged currents. The allowed regions are those which include $\alpha = \zeta = 0$. Muon-decay contours are derived from decay-rate measurements at the spectrum end point (bold curve, this experiment); the polarization parameter ξP_μ (dotted curve, Ref. 4); and the Michel parameter ρ (solid curves, Ref. 5). Nuclear β -decay contours are obtained from the Gamow-Teller β polarization (dot-dashed curves, Ref. 6); the comparison of Gamow-Teller and Fermi β polarizations (long-dashed curves, Ref. 7); and the ^{19}Ne asymmetry $A(0)$ and $f t$ ratio, with the assumption of conserved vector current (short-dashed curves, Ref. 8). Limits from the y distributions in νN and $\bar{\nu} N$ scattering (double lines, Ref. 9) are valid irrespective of the ν_R mass.

strains both α and ζ .

This experiment is made possible by the nearly complete polarization of a μ^+ beam derived from π^+ decay at rest near the surface of the production target.¹² The M13 beam¹³ at the Tri-University Meson Facility (TRIUMF) cyclotron produces 15 000 29.5-MeV/c μ^+ per sec within a 1% $\Delta p/p$ and a 12×10 -mm spot. The 2% contamination of prompt ("cloud") μ^+ from π^+ decay in flight is rejected by requiring the μ^+ to be produced well within the 43-nsec interval between proton bursts.

The apparatus is shown in Fig. 2. After traversing 50 mg/cm², beam μ^+ are stopped by target foils of $\geq 99.99\%$ -pure Al (155 mg/cm²), Cu (233 mg/cm²), Ag (275 mg/cm²), and Au (233 mg/cm²). The high free-electron concentration in these metals screens the stopped μ^+ from prolonged spin-spin coupling to particular electrons, which otherwise would lead to its depolarization. A 1.1-T longitudinal field (B_{\parallel}) is also applied to preserve the stopped μ^+ spin direction. During alternate hourly runs the longitudinal field is nulled to within ± 3 G and a 70-G transverse field (B_{\perp}) is substituted. This precesses the μ^+ spin about a

vertical axis so that its time-averaged polarization is zero. Downstream of the target the decay e^+ is focused by a 0.5-T·m solenoidal field lens. The septum between the target and solenoid bore decouples the focal length from the target field orientation.

The decay e^+ is momentum analyzed by an NMR-monitored cylindrical dipole magnet having a central field of 0.32 T. Low-mass drift chambers using methane gas are located near its conjugate foci, and the intervening volume is evacuated. The dispersion $\Delta p/p$ was measured to be 1.07%/cm by passing e^+ beams of different momenta through the spectrometer. The combined system of field lens and positron spectrometer has an acceptance of 250 msr and a momentum bite of $\pm 20\%$; in the analysis described below, these were restricted to 160 msr and $\pm 8\%$.

The trigger requires the signature of a beam particle stopping in the foil target, in delayed (0.2–10 μ sec) coincidence with that of a decay positron passing through the spectrometer. Events with an extra beam particle arriving between the μ^+ stop and decay are tagged and rejected later. The data reported here are based on 3.5×10^6 triggers from the initial run. (An additional 10^7 triggers were collected later.)

Incoming μ^+ tracks were reconstructed with use of P1 and P2. Nearly straight e^+ track segments were found separately in the horizontal and vertical projections of three groups of wire chamber planes: (P3, D1, D2); D3; and D4 (Fig. 2). All possible combinations of hits were considered, and tracks in all six segments were found in 99% of the triggers. Of these, 95% had hit multiplicities corresponding to a single track; the remainder were rejected. Projections of the track segments were required to agree at the target, in the bore of the solenoid, and in position and vertical slope in the dipole. Track segment residuals were used to dynamically fine-tune the drift-chamber space-time calibration, producing residuals of ≤ 250 μ m in the spectrometer chambers D3 and D4.

The hits found in P1 through D2 were then fitted to curved trajectories based on the first-order optics of cylindrically symmetric fields. The μ^+ and e^+ polar angles θ_{μ} and θ_e with respect to the beam axis at the target were thereby determined with resolutions of 20 and 10 mrad, respectively. Monte Carlo simulation based on higher-order field optics confirms the accuracy of this procedure to within an uncertainty of ± 0.0005 in $\cos\theta_{\mu}$ and $\cos\theta_e$. For the B_{\parallel} data the transverse com-

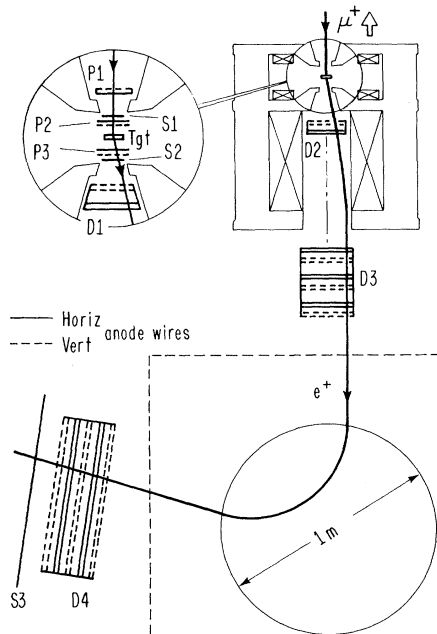


FIG. 2. Plan view of muon polarimeter. P1–P3 are proportional wire chambers, D1–D4 are drift chambers, and S1–S3 are scintillators. The trigger is $T1 \cdot T2$, where $T1$ is $P1 \cdot S1 \cdot P2 \cdot \bar{V}1 \cdot \bar{P}3 \cdot S2$ at the μ^+ stopping time, $T2$ is $P3 \cdot S2 \cdot S3 \cdot \bar{P}1 \cdot S1 \cdot \bar{V}1 \cdot \bar{P}2 \cdot \bar{V}2$ at the μ^+ decay time, and $V1$ and $V2$ are veto scintillators surrounding S1 and S2, respectively (not shown).

ponent of the μ^+ spin precesses about the beam axis too rapidly to be followed. Thus for $\cos\theta = -\hat{P}_\mu \cdot \hat{p}_e$ in Eq. (1) we substitute $\cos\theta_\mu \cos\theta_e$, which is equivalent in an average over many events.

The e^+ momentum was obtained by taking the sum of the horizontal coordinates at the conjugate foci of the 98° horizontally focusing spectrometer magnet. With use of the momentum, deviation from the median plane, and impact parameter with respect to the magnet axis as parameters, this sum was empirically corrected to second order, based primarily on the end-point position in B_\perp data. The sharp edge at $x=1$ in Fig. 3, curve *a* exhibits a Gaussian resolution which is less than 0.2% rms, with a rounded shoulder due to straggling in the 180 mg/cm² of material upstream. We have dropped events with $x < 0.92$ and $\cos\theta < 0.975$, which have low statistical power. After conservative fiducial cuts the final distributions in Fig. 3 retain 7.5% of the raw triggers. We have checked that any reasonable variation of the cuts would negligibly affect the result.

Fitting proceeds in two stages. The B_\perp data in Fig. 3, curve *a* are fitted to the radiatively cor-

rected spectrum expected¹¹ for unpolarized μ^+ decay, smeared by a sum of Gaussian resolution functions and by the expected e^+ energy-loss straggling. The B_\parallel spectrum in Fig. 3, curve *b* can be represented as the shape expected from pure $V-A$ and $P_\mu = \cos\theta = 1$, with a small admixture of the unpolarized spectrum in Fig. 3, curve *a*. This unpolarized fraction is essentially equal to $1 - (\xi P_\mu \delta/\rho) \langle \cos\theta \rangle$. To fit this fraction, we use the B_\perp fit to fix the x resolution, x acceptance, and edge position $x=1$, but allow the acceptance for B_\parallel data relative to that for B_\perp data to vary linearly with x . This allows for the (<2%) difference in angular acceptance caused by the different field configuration near the target. Using data with partly polarized cloud μ^+ , we have checked that the $x=1$ calibration is consistent for B_\parallel and B_\perp fields. In the resulting curve in Fig. 3, curve *b*, the slight kink near $x=1$ reflects the small fitted unpolarized fraction, which arises mostly from the measured value $\langle \cos\theta \rangle = 0.9862$ for these data.

The result reported here is based on this same fitting procedure carried out for data in each of five bins in $\cos\theta$. The subdivision checks that the results of these fits are consistent with a linear dependence upon $\langle \cos\theta \rangle$. Separate fits for each of the four stopping-target materials give values of $\xi P_\mu \delta/\rho$ which are statistically consistent ($\chi^2 = 2.1$), with a combined statistical error of ± 0.0015 . Within statistical errors the result is also independent of the time of muon decay.

Because the measured values of $\cos\theta_\mu \cos\theta_e$ are systematically too high as a result of Coulomb scattering in the production and stopping targets, an estimated correction of $+0.0012 \pm 0.0005$ has been applied to all fitted $\xi P_\mu \delta/\rho$. Table I sum-

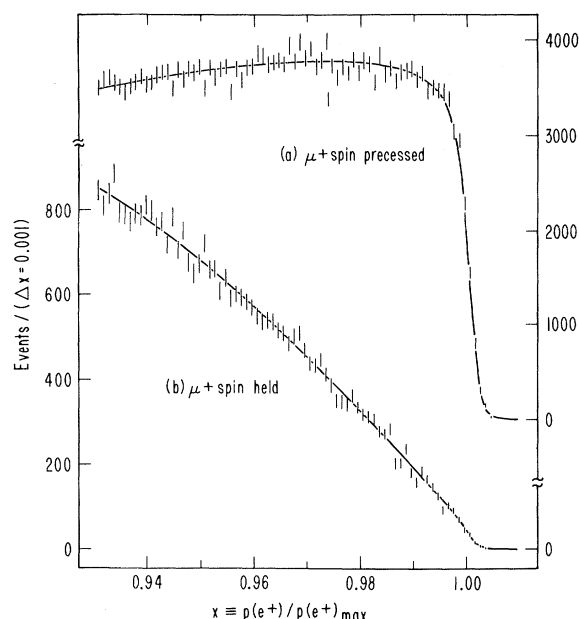


FIG. 3. Distributions (uncorrected for acceptance) in reduced positron momentum with the μ^+ spin precessed (curve *a*) and held (curve *b*). Errors are statistical. The edge in curve *a* corresponds to a resolution with a Gaussian part <0.2% rms. The fits are described in the text.

TABLE I. Major sources of systematic error and their estimated contributions.

Source of systematic error	Error
Coulomb scattering in targets	± 0.0005
Correction of θ_μ and θ_e for bending in B_\parallel field at target	± 0.0010
Smearing of θ_μ and θ_e due to detector resolution and scattering	± 0.0006
Possible shift in θ_e due to random hits and inefficiencies in D1 and D2	± 0.0005
Method of averaging $\langle \cos\theta \rangle$	± 0.0004
Difference in $x=1$ edge calibration between B_\perp and B_\parallel data	± 0.0008
Normalization of B_\parallel relative to B_\perp data	± 0.0007

marizes the major sources of systematic error. All other sources contribute less than 10^{-4} . In principle the systematic errors should not be correlated; in quadrature they add to ± 0.0018 . We have made no correction for unknown sources of μ^+ depolarization either along the beam or in the stopping target. Since such effects can only decrease the apparent result, we therefore quote the limit $\xi P_\mu \delta / \rho > 0.9959$ (90% confidence). The corresponding limits on the mass and mixing parameters α and ξ are represented by the small bold contour in Fig. 1. In particular, for infinite W_R mass $|\xi| < 0.045$; for any mixing angle $M(W_R) > 380$ GeV; and for zero mixing angle $M(W_R) > 450$ GeV.

We are indebted to the entire TRIUMF management and staff for their splendid support of this experiment. In its early stages we benefited from discussions with J. Brewer, R. Cahn, K. Crowe, K. Halbach, and W. Wenzel, and from the technical contributions of C. Covey, R. Fuzesy, F. Goozen, P. Harding, M. Morrison, and P. Robrish. This research was supported in part by the U. S. Department of Energy through Contracts No. DE-AC03-76SF00098 and AC02-ER02289.

^(a)Present address: Department of Physics, Northwestern University, Evanston, Ill. 60201.

^(b)Present address: Tri-University Meson Facility, Vancouver, B.C. V6T 2A3, Canada.

¹J. C. Pati and A. Salam, Phys. Rev. Lett. **31**, 661 (1973), and Phys. Rev. D **10**, 275 (1974); R. N. Mohapatra and J. C. Pati, Phys. Rev. D **11**, 566, 2588 (1975).

²M. A. B. Bég *et al.*, Phys. Rev. Lett. **38**, 1252 (1977). The present measurement assumes $M(\nu_R) = 0$ and is insensitive to W_R effects beyond $M(\nu_R) = 10$ MeV.

³B. R. Holstein and S. B. Treiman, Phys. Rev. D **16**, 2369 (1977).

⁴The primary input to the world average is V. V. Akhmanov *et al.*, Yad. Fiz. **6**, 316 (1967).

⁵The primary input to the world average is J. Peoples, Nevis Cyclotron Report No. 147, 1966 (unpublished).

⁶J. Van Klinken, Nucl. Phys. **75**, 145 (1966).

⁷J. Van Klinken *et al.*, Phys. Rev. Lett. **50**, 94 (1983).

⁸D. Schreiber and F. T. Calaprice, private communication; D. Schreiber, Ph.D. thesis, Princeton University, 1983 (unpublished). We calculated the contour plotted in Fig. 1 using $A(0) = 0.0363 \pm 0.0008$; ft ratio $= 1.797 \pm 0.002$. See also F. T. Calaprice *et al.*, Phys. Rev. Lett. **35**, 1566 (1975).

⁹H. Abramowicz *et al.*, Z. Phys. C **12**, 225 (1982).

¹⁰G. Beall, M. Bander, and A. Soni, Phys. Rev. Lett. **48**, 848 (1982) find $M(W_R) > 1600$ GeV; P. DeForcrand, Ph.D. thesis, University of California, Berkeley, 1982, Lawrence Berkeley Laboratory Report No. LBL-14692 (unpublished) finds $M(W_R) > 200$ GeV.

¹¹F. Scheck, Phys. Lett. **44C**, 187 (1978); A. M. Sachs and A. Sirlin, in *Muon Physics*, edited by V. Hughes and C. S. Wu (Academic, New York, 1975), Vol. 2, p. 50.

¹²A. E. Pifer *et al.*, Nucl. Instrum. Methods **135**, 39 (1976).

¹³C. J. Oram *et al.*, Nucl. Instrum. Methods **179**, 95 (1981).